Journal of Nano- and Electronic Physics
Vol. **10** No 6, 06002(6pp) (2018)

Журнал нано- та електронної фізики
Том **10** № 6, 06002(6cc) (2018)

Computer Modeling Zinc Oxide/Silicon Heterojunction Solar Cells

N. Ziani*, M.S. Belkaid

Laboratory of Advanced Technologies of Genie Electrics (LATAGE), Department of Electronics, Mouloud Mammeri University (UMMTO), Tizi-Ozou, Algeria

(Received 29 August 2018; revised manuscript received 01 December 2018; published online 18 December 2018)

A new type of solar cells – Zinc Oxide/Silicon (ZnO/Si) hetero-junction are explored for their potentially low cost application. In order to find the optimal design structure of ZnO/*p*-Si solar cells, numerical modeling using SCAPS-1D (Solar Cell Capacitance Simulator One Dimension) is performed. We study the most important quality parameters, their variations and their impacts on performances of solar cells. The thickness of emitter and buffer layers is varied to observe its effect on the cell performance. Thus, the defects located in ZnO and Si layers, as well as, the role of the of interface defects' density of the ZnO/*c*-Si heterojunction solar cells have been investigated in detail to provide guidelines for achieving high performance. The results indicate that the cell with an optimum thin buffer layer has higher performance. Also the output characteristics of these cells are significantly more sensitive to the defects in silicon surface than ZnO surface. The results also show that the interface defect states have an obvious effect on the open circuit voltage of these cells. We argue that the conversion efficiency of ZnO/*c*-Si heterojunction solar cells could be increased beyond 17 % by efficiently regulating interface Dit and defects in silicon layer.

Keywords: Modeling, Solar cells, ZnO/Si heterojunctions, Thickness, Defect densities.

DOI: 10.21272/jnep.10(6).06002 PACS numbers: 78.20.Bh, 73.40.Lq, 84.60.Jt

1. INTRODUCTION

Among different kinds of solar cells, *p*–*n* junction solar cells based on c-Si wafers are undoubtedly favored as they allow solar cells with efficiencies above 20 % [1-3]. However, *c*-Si based solar cells require high manufacturing cost [1]. Therefore, reducing the cost becomes a major issue, which attracts much attention. Recent research shows that depositing transparent conductive oxide (TCO) on *c*-Si substrates becomes an effective way to overcome these limitations [4-8]. Among all those TCO materials, there has been increasing interest in zinc oxide (ZnO) films due to their superior electrical and optical properties in combination with low resistivity and high optical transparency (> 80 %) to visible light [9-13].

Intrinsically, ZnO is an *n*-type material due to the number of defects introduced during the growth, irrespective of growth method. These defects are commonly believed to be Zn interstitial and oxygen vacancy [14]. However, *n*-type conductivity of ZnO can be very beneficial to the current thick film Si solar cell fabrication. The emitter of a silicon solar cell is made by a high temperature and long diffusion of phosphorus into the bulk silicon to form a *pn* junction. ZnO can be an alternative to the emitter formation by phosphorus because of high *n*-conductivity as well as antireflection coating. This will remove the high temperature diffusion step from the current Si solar cell fabrication process.

In recent years, ZnO has drawn global research interest due to its unique conductive, piezoelectronic and optoelectronic properties. These promising properties such as wide band gap (3.37 eV), large exciton binding energy (~ 60 meV), large saturation energy and high thermal and mechanical stability makes it a suitable choice for photodetectors, solar cells, light emitting diodes, sensors and piezoelectronic devices [15-17]. With a wide band gap, high transparency and low resistivity material, it can be used as a window layer and simultaneously heterojunction partner for heterojunction based solar cells [18-23]. Using ZnO over Si provides a window for photon transfer, gives a higher built in potential to increase the open circuit voltage *Voc* and to passivate the surface and grain boundary defects to reduce the dark current [19]. Note that the *n*-ZnO/*p*-Si heterojunction solar cells, the solar light (the visible spectrum and near infrared) can be efficiently collected owing to the wide band gap of ZnO (*Eg* = 3.3 eV).

There are many researches on ZnO/*c*-Si heterojunction solar cells. For example, without interface states density, Babar et al reported with simulation of n-ZnO/*p*-Si solar cell a conversion efficiency of ~ 19 % [2] and Zeng et al fabricated B:ZnO/Si solar cell and reach a *Voc* of 628 mV, *Jsc* of 41 mA. Cm^{-2} and efficiency of 17.78 % [24]. Gluba et al reported the growth of ZnO/*p*-Si structure by Pulsed Laser Deposition (PLD) with excellent interface passivation due to trap density reduction from 10^{12} to 10^{11} cm^2 [25]. Baturay et al reported good rectifying junction properties by Gallium doping of ZnO grown on Si [26]. Pietruszka et al showed that the incorporation of Magnesium (Mg) into ZnO with Atomic layer deposition (ALD) method at low temperature, can lead to the improved interface with Si for solar cell fabrication [6]. Belaid et al have studied the effect of In doped ZnO/Si solar cells and showed improved performance compared to undoped ZnO/Si solar cells [27].

The performance of the heterojunction cell strongly depends on the doping concentration, the bulk defect density and the respective thicknesses of *n*-ZnO and *p*-Si layers. Indeed, modifying their properties affects both charge carrier transport at the junction (recombination, field effect) and photogeneration. Mostly, the bulk defects within the ZnO film and defects/traps at

* nziani14@gmail.com

the interface of ZnO/Si layers [28] have blame for poor photovoltaic performance. In this paper, device modeling and numerical simulations of ZnO/Si solar cells are performed to analyze the influence of (a) the buffer and emitter layers thickness, (b) the defect states in the Si absorption layer and those in the ZnO emitter layer and (c) the ZnO/*c*-Si interface defect state density on the solar cell characteristics.

2. MODELING

Numerical Modeling has been increasingly used as a tool to understand the physical operation of the solar cells. Various measurements are done to understand the optical and electrical properties of the solar cell. However, it is difficult to analyze these measurements without the precise model. Therefore, numerical modeling is necessary to interpret the advanced measurement on complicated structures, design and optimization of advanced cell structures. Following are the most important things to consider in simulation software: Capability of solving the basic equations – Poisson equation and the continuity equation for electron and hole. The simulation program for proposed ZnO/*p*-Si heterojunction solar cell structure has been developed in SCAPS simulator to obtain various electrical and optical characteristics. SCAPS-1D (a solar cell capacitance simulator in one dimension) is written and maintained at the University of Gent [29]. It is mainly used for modeling CdTe, CIS and CIGS based thin film solar cells. SCAPS-1D solves the one dimensional semiconductor equations. The three equations read:

$$F_1\left(\psi, E_{fn}, E_{fp}\right) = \frac{\partial D}{\partial x} = +q\left(p - n + N_D - N_A + p_t - n_t\right) \quad (1)$$

$$F_2\left(\psi, E_{fn}, E_{fp}\right) = \frac{\partial J_n}{\partial x} = -q\left(G - R_n\right) \quad (2)$$

$$F_3\left(\psi, E_{fn}, E_{fp}\right) = \frac{\partial J_p}{\partial x} = +q\left(G - R_p\right) \quad (3)$$

where, ψ – electrostatic potential, E_{fn}, E_{fp} – quasi-Fermi level for electron and hole respectively, D is the displacement field. p, n – hole/electron densities. p_t – net charge, N_D, N_A – donor and acceptor impurity concentration respectively, J_n, J_p – electron and hole current density respectively, G – optical generation rate, R_n, R_p – electron and hole recombination rates.

Recombination in deep bulk levels and their occupation has been described by the Shockley-Read-Hall (SRH) formalism. Recombination at the interface states is described by an extension of the SRH formalism, which allows the exchange of electrons between the interface state and the two adjacent conduction bands, and of holes between the state and the two adjacent valence bands. Conduction band discontinuity, valence band discontinuity, effective density of states for electrons in the conduction band and holes in the valence band respectively, separation between Fermi levels and band gap edges in *p*- and *n*-type regions (δp, δn) are calculated during the simulation using the following equations:

$$\Delta Ec = \chi_{ZnO} - \chi_{Si} \quad (4)$$

$$\Delta E_V = (E_{gZnO} - E_{gSi}) - \Delta Ec \quad (5)$$

$$N_c = 2\left(\frac{2\pi m_e^* KT}{h^2}\right)^{\frac{3}{2}} \quad (6)$$

$$N_v = 2\left(\frac{2\pi m_h^* KT}{h^2}\right)^{\frac{3}{2}} \quad (7)$$

$$\delta_p = \frac{KT}{q} ln \frac{N_A}{N_V} \quad (8)$$

$$\delta_n = \frac{KT}{q} ln \frac{N_D}{N_C} \quad (9)$$

where χ_{ZnO}, χ_{Si} – electron affinity for ZnO and Si, E_{gZnO}, E_{gSi} – band gap of ZnO and Si, respectively, m_e*, m^*_h – effective mass of electron and holes, k – Boltzmann constant, T – lattice temperature and q is the charge of electron.

The heterostructures have been treated with the affinity rule to divide the difference in band gap. Transport across the interfaces is modeled with thermionic emission. The modeled structure is shown in Fig. 1. The first layer represents doped ZnO. The second layer is either identical to the first one or it represents an intrinsic ZnO buffer layer. The defect states of ZnO principally consist of acceptor like and donor like defect states, which are both single distribution. For the crystalline absorber a *p*-type *c*-Si is set 200 μm thick with doping concentration of 1×10^{16} cm^{-3}. It is characterized by a single donor-type defect centered at mid-gap with a density of 5×10^{11} cm^{-3} and the capture cross section for holes and for electrons is equal to 10^{-8} cm^2. The front side of the crystalline silicon is modeled by a defect rich surface layer with defect state densities varying from 1×10^9 cm^{-3} to 2×10^{14} cm^{-3}. At the rear side a highly doped back surface field layer (10^{17} cm^{-3}) is assumed. Interface properties have further been studied by introducing acceptor traps (single

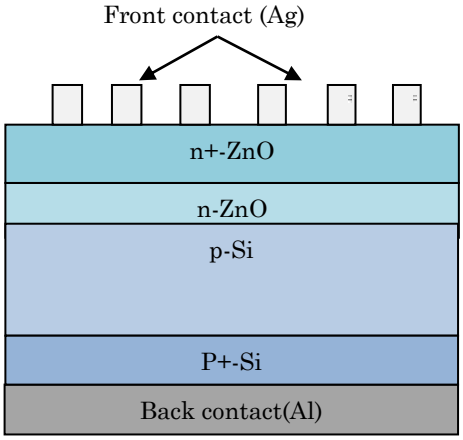

Fig. 1 – Structure used for modeling the ZnO/*p*-Si heterojunction

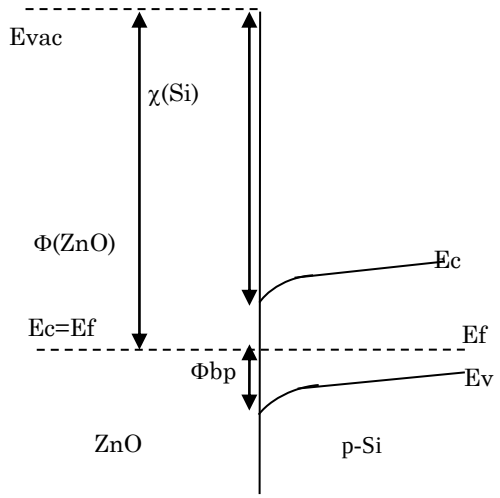

Fig. 2 – Band structure of ZnO/Si(*p*) heterojunction solar cell

energy level at 0.3 eV below the conduction band) [19], with the capture cross sections of electron and hole both at 10^{-12} cm^2, at the heterointerface of ZnO buffer layer and Si substrate. Fig. 2 shows the energy band diagram for ZnO/Si heterostructure. Light is assumed to be falling from the top of the heterojunction. Table 1 shows set of parameters that has been taken into consideration for the simulation of heterojunction cell. The temperature is set to 300 K by accepting the default value.

3. RESULTS AND DISCUSSION

In these section simulation results of ZnO/*p*-Si heterostructure solar cells has been presented. The J-V characteristics under illumination, at the spectrum of Air Mass 1.5 used in the SCAPS software modeling tool is shown in Fig. 4. The ZnO/Si junction can be approximated as a metal-semiconductor junction with a depletion region occurring mainly in the Si substrate. Simulated energy band diagram of ZnO/*p*-Si heterojunction is illustrated in Fig. 3.

3.1 Effect of Emitter Layer Thickness on Cell Performance

Front and back contacts were assumed as flat band and surface recombination velocities were set as 1.0×10^7 cm s^{-1}. ZnO emitter thickness is varied from 100 nm to 500 nm. Fig. 5 shows the output characteristics of ZnO/Si(*p*) solar cell as a function of ZnO emitter thickness.

Table 1 – Modeling parameters used in the simulation

	n-ZnO	*i*-ZnO	*p*-Si
Layer thickness	100-500 nm	20-50 nm	200 μm
Electron affinity (eV)	4.65	4.65	4.05
Electron mobility (cm^2/V·s)	100	100	1500
Hole mobility (cm^2/V·s)	2500	2500	480
Band gap (eV)	3.37	3.37	1.12
Effective density of states in the conduction band Nc (cm^{-3})	2.8×10^{19}	2.8×10^{19}	2.8×10^{19}
Effective density of states in the valance band Nv (cm^{-3})	2.8×10^{19}	2.8×10^{19}	1.04×10^{18}
Doping concentration (cm^{-3})	1×10^{19}	0	1×10^{16}
Dielectric constants (ε)	8.5	8.5	11.9
Hole capture cross (cm^2)	10^{-10}	–	10^{-8}
Electron capture cross (cm^2)	10^{-10}	–	10^{-8}

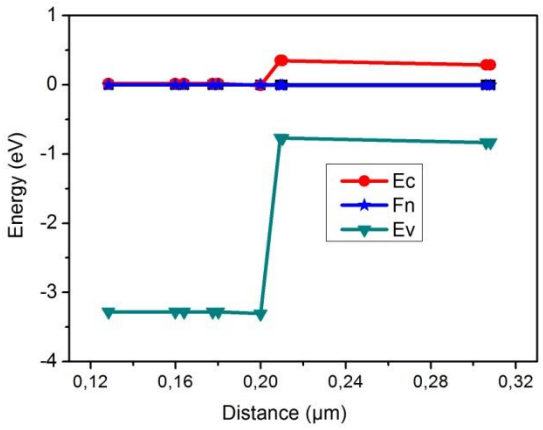

Fig. 3 – Simulated energy band diagram of ZnO/Si solar cell

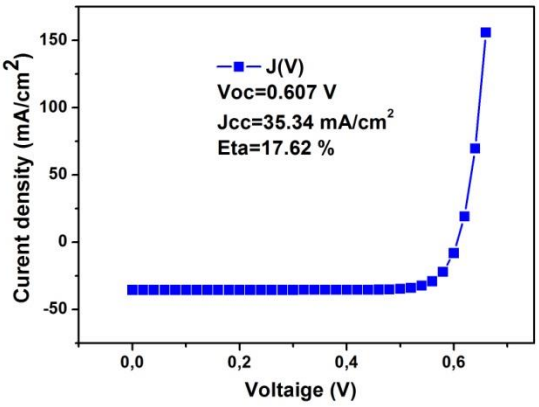

Fig. 4 – J-V characteristic of ZnO/Si heterojunction device measured at the AM1.5

From Fig. 5a, we can be seen that the emitter thickness increases, the open circuit voltage and the short circuit current density decreases slightly around 0.79 mV and 0.49 mA·cm^{-2} in the range of 100 nm to 500 nm. This is due to the increasing of the absorption of the photon in the thicker emitter. However, due to the absence of electric field in the emitter and at presence of recombination centers, the photo-generated porter can not to arrive the edge of the space charge region and participate to the light current. They recombined in the region and disappear, resulting in the reduced short-circuit current density. In the low thicknesses, the fill factor increase, when the thickness is larger than 250 nm, FF considered constant (Fig. 5b). Due to the decrease of *Voc* and *Jsc*, the efficiency (η) decrease with emitter layer thickness. Taking into account the technical production and conversion efficiency, the emitter thickness should be chosen at about 100 nm.

3.2 Effect of Buffer Layer Thickness on Cell Performance

The zinc oxide buffer layer is introduced between the doped zinc oxide and the crystalline silicon; the role of the buffer layer is to reduce density of defect states, therefore reduced the interface recombinaison.

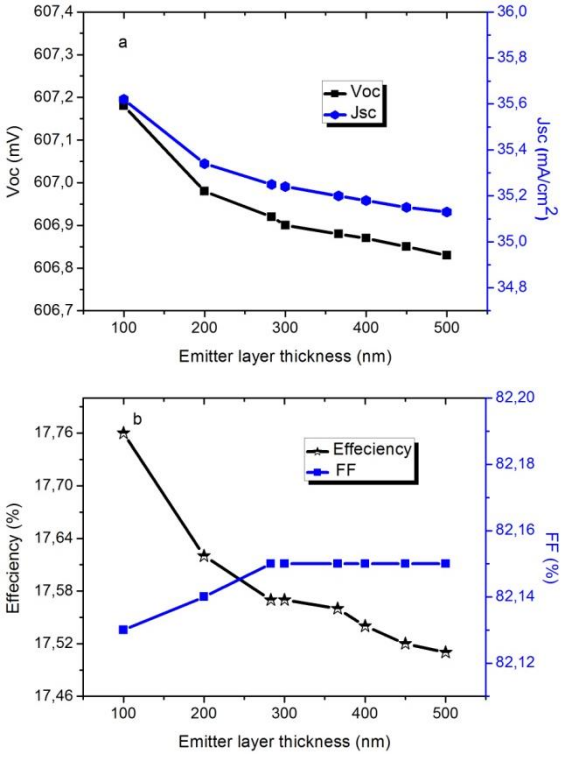

Fig. 5 – Simulated performances (a) *Jsc*, *Voc* and (b) efficiency, FF of ZnO/*c*-Si(*p*) solar cells as a function of ZnO emitter layer thickness

In order to evaluate the buffer layer thickness effect, on the ZnO/*p*-Si heterojunction solar cell properties, we vary the thickness in our simulation from 10 nm to 50 nm as shown in Fig. 6. As can be seen, with the increase of the buffer layer thickness, the short circuit current density of the cell decreases, resulting in the reduced efficiency and fill factor. This is mainly because, more photons will be absorbed in the thicker interlayer and fewer photons can achieve the absorber layer, consequently, the recombination at the buffer layer enhances. The variation of the open circuit voltage is insignificant when the buffer layer thickness increases.

Counterbalancing the production processes and the conversion efficiency, the optimal intrinsic layer thickness should be set at 20 nm.

3.3 Effect of Emitter and Absorber Defect Density on Cell Performance

Then, in this section, we try to find out how the defect layer influences the performance. After the optimization of cell thickness without defects state, the photovoltaic parameters by assuming the defects in the region *p*-Si and *n*-ZnO have been calculated. Effects of defect state in p-Si and *n*-ZnO are shown in Fig. 7 and Fig. 8. As can be seen from the Fig. 7, V_{oc} is reduced from 600 to 420 mV and as the total density of defect states increases, and thus, the efficiency is reduced. However, these defects create energy levels in the gap of Si layer which causes the recombination of free carriers, and reduces the conversion efficiency of the solar cell. We observed that the conversion efficiency η decrease with increasing the defects density in *p*-Si layer.

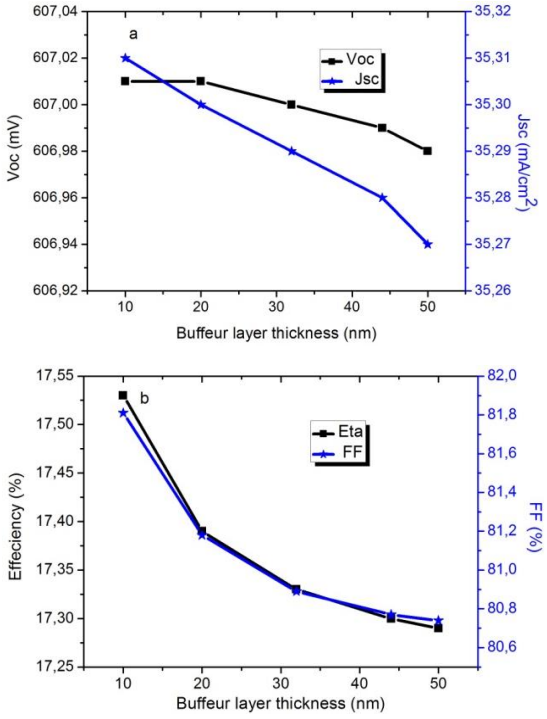

Fig. 6 – Variation of (a) *Jsc*, *Voc* and (b) efficiency, FF of the solar cell with the buffer layer thickness

Fig. 8 illustrates the dependence of the *n*-ZnO defect density on cell performance. When the defect density is varied from 10^{11} to 10^{17} cm^{-3} in *n*-ZnO layer, we observed that the defects have negligible impact on *Jsc*, *Voc*, η and FF.

Those defects could be affected by a combination of defect density, defect capture cross section, and defect location. We can conclude that the performances of these cells are sensitive to the defects in silicon surface.

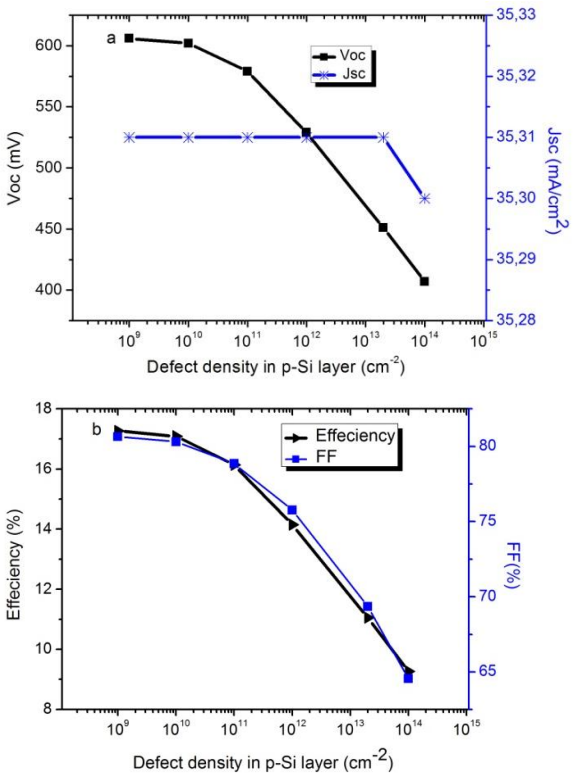

Fig. 7 – Variation of (a) *Jsc, Voc*, and (b) Efficiency, FF in *n*-ZnO/*p*-Si device as a function of defects density in *p*-Si layer

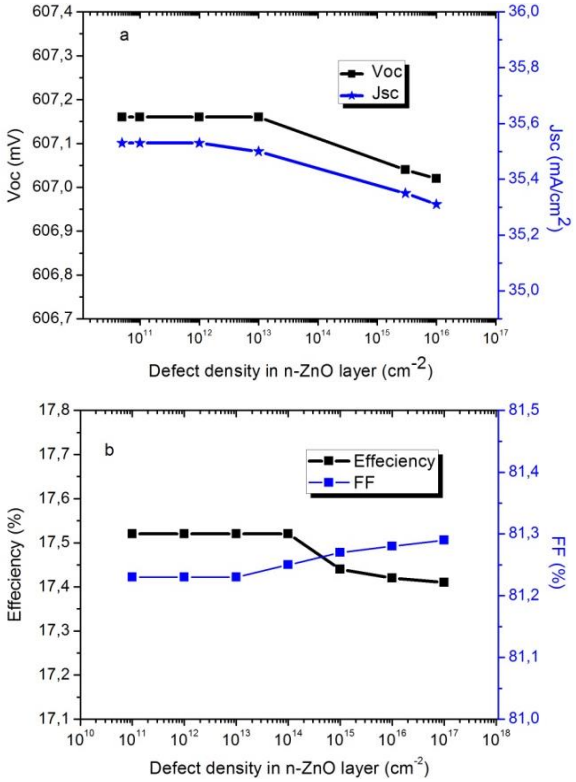

Fig. 8 – Variation of (a) *Jsc, Voc* and (b) Efficiency, FF in n-ZnO/*p*-Si device as a function of defects density in *n*-ZnO layer

3.4 Effect of Interface Defect States on Cell Performance

In order to study the influence of interface state density on *n*-ZnO/i-ZnO/*p*-Si characteristics, the interface state densities (Dit) between *i*-ZnO and *p*-Si layers were varied, in the simulations, from the range of 1×10^8 to 1×10^{13} cm^{-2}. Fig. 9 displays the simulated values of *Voc, Jsc*, FF and efficiency at various interface state densities. Our calculation showed that by increasing the interface state density (D_{it}), the short circuit current density and open circuit voltage decreases as shown in Fig. 9a. In the lower value of interface states, recombination current has minimum value and also *Jsc* is not sensitive to the defect state. By increasing the D_{it} from 1×10^{12} cm^{-2} to 1×10^{13} cm^{-2}, *Jsc* decreases from 35.29 mA·Cm^{-2} to 34.82 mA·Cm^{-2}, *Voc* decreases sharply from 165 mV to 44 mV, and thus, the efficiency is reduced. So, the large recombination via the interface defects degrades the solar cell performances.

The interface defects affect mostly the open circuit voltage, this can be expressed by the following relationship 10:

$$V_{oc} = \frac{1}{q}\left\{\varnothing_B - nKTLn\left(\frac{qN_vS_{it}}{J_{sc}}\right)\right\} \qquad (10)$$

where ϕ_B represents the effective barrier height, n the ideality factor and S_{it} the interface recombination velocity (deduced from D_{it}).

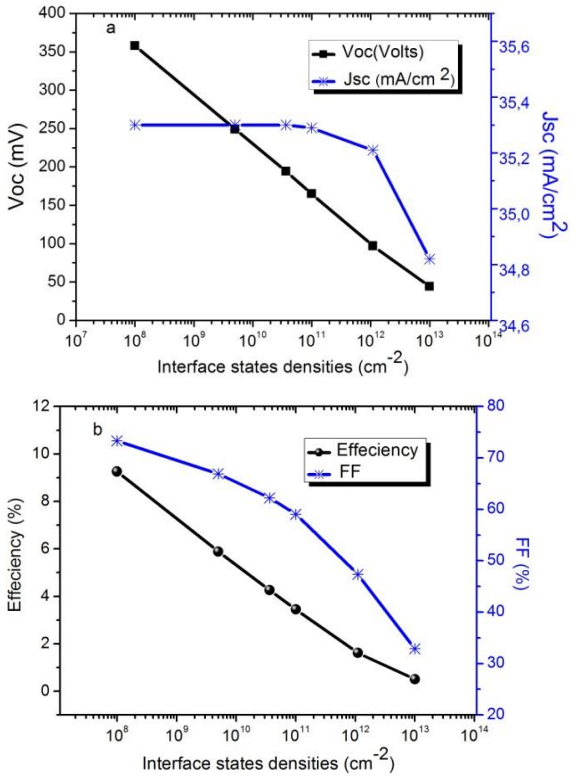

Fig. 9 – Simulated performances of ZnO/*c*-Si(*p*) heterojunction solar cells as a function of interface state densities

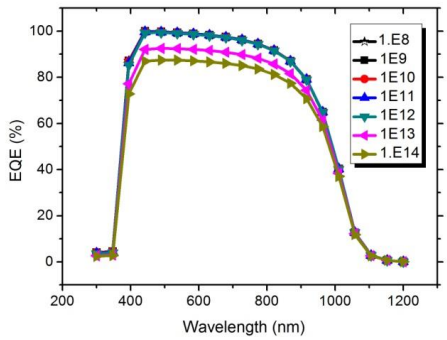

Fig. 10 – Dependence of spectral response of the device with interface state densities

Furthermore, Fig. 10 shows the external quantum efficiency (EQE) of the device with different interface states. All the cells demonstrate difference over a wide range of wavelength from 300 nm to 1200 nm. The higher interface states give a noticeably decreased response in the visible spectrum. It indicates that the carriers generated in the absorber layer are mainly got recombination. However, in presence of interface defects, more photons are being absorbed by the interface states; fewer photons can contribute to the quantum efficiency and, consequently, the spectral response decreases.

We notice that the cell efficiency (η) and fill factor (FF) obtained for different values of D_{it} reflects more or less the same nature as *Jsc* and *Voc*.

4. CONCLUSION

This work attempts to indentify the optimal device design and the performance properties of ZnO/*p*-Si heterojunction solar cells. Modeling the ZnO/*p*-Si solar cell structures on SCAPS gives an optimal design strategy. The results show that optimal ZnO layer should have a thin thickness of 100 nm. Due to the nature of heterojunctions, defects are very easily formed at the junction interface. The ZnO/*p*-Si solar cell simulation with high interface defects was also performed. We observe that the efficiency of the cell depends heavily on the interface defects density. Comparing the SCAPS-1D simulation using defect density in Si layer and in ZnO layer, the output characteristics of these cells are sensitive to the defects in silicon surface more than the ZnO surface. Those defects are affected by a combination of defect density, defect capture cross section and defect location.

The ZnO/*p*-Si based heterojunction solar cell appears to be an interesting alternative regarding the performance efficiency. This is due to its simple and low temperature processing steps which makes of it a low cost candidate.

AKNOWLEDGEMENTS

We gratefully acknowledge to Dr. Marc Burgelman, University of Gent, Belgium, for providing the opportunity to use SCAPS-1D simulation software.

REFERENCES

1. F. Chaabouni, M. Abaab, B. Rezig, *Super. Lattices. Microstruct* **39**, 171 (2006).
2. B. Hussain, A.Ebong, I. Ferguson, *Sol. Energy Mater. Sol. C* **139**, 95 (2015).
3. G. Wang, Z. Li, S. Lv, M. Li, C. Shi, J. Liao, H. Chen, *Ceram. Int.* **42**, 2813 (2016).
4. W. Chebil, A. Fouzri, A. Fargi, B. Azeza, Z. Zaaboub, V. Sallet, *Mater. Res. Bull.* **70**, 719 (2015).
5. M. Soylu, O. Savas, *Mater. Sci. Semicond. Proc.* **9**, 76 (2015).
6. R. Pietruszka, R Schifano, T.A. Krajewski, B. S. Witkowski, K. Kopalko, L. Wachniki, E. Zielony, K. Gwozdz, P. Bieganski, E. Placzek-Popko, M. Godlewski, *Sol. Energy Mater. Sol. C.* **147**, 164 (2016).
7. R. Balasundaraprabhua, E.V. Monakhov, N. Muthukumarasamy, O. Nilsen, B.G. Svensson, *Mater. Chem. Phys.* **114**, 425 (2009).
8. A.A. Ibrahim, A. Ashour, *J. Mater. Sci. Mater. Electron.* **17**, 835(2006).
9. J.D. Ye, S.L. Gu, S.M. Zhu, W. Liu, S.M. Liu, R. Zhang, Y. Shi, Y.D. Zheng, *Appl. Phys. Lett.* **88**, 182112 (2006).
10. D. Song, A.G. Aberle, J. Xia, *Appl. Surf. Sci.* **195**, 291 (2002).
11. H. Belkhalfa, H. Ayed, A. Hafdallah, M.S. Aida, R. Tala Ighil, *Optik* **127**, 2336 (2016).
12. S. Mridha, M. Dutta, D. Basak, *J. Mater. Sci. Mater. Electron* **20**, 376 (2009).
13. W. Zhang, Q. Meng, B. Lin, Z. Fu, *Sol. Energy. Mater. Sol. C.* **92**, 949 (2008).
14. M.D. McCluskey, S.J. Jokela, *J. Appl. Phys.* **106**, 071101 (2009).
15. K.B. Sundaram, Ashamin Khan, *J. Vac. Sci. Tech. A.* **15**, 428 (2009).
16. K.R. Romero, M.C. Lopez, D. Leinen, F. Martin, J.R. Ramos-Barrado, *Mater. Sci. Eng. B* **110**, 87 (2004).
17. R. Ghosh, D. Basak, *Appl. Phys. Lett.* **90**, 243106 (2007).
18. H.H. Afify, S.H. EL-Hefnawi, A.Y. Eliwa, M.M. Abdel, N.M. Ahmed, *Egypt. J. Solids.* **28**, 243 (2005).
19. T. Yen, M. Li, N. Chokshi, R.L. De Leon, J. Kim, G. Tompa, W.A. Anderson, *4th photovoltaic energy conversion conference*, 1653(2006).
20. D.G. Baik, S.M. Cho, *Thin Solid Films* **354**, 227 (1999).
21. Z.W. Ying, Z. Sheng, S.L. Jie, F.Z. Xi, *Chin. Phys. Lett.* **25**, 1829 (2008).
22. A. Ali, B. Hussain, A. Ebong, *IEEE 43rd Photovoltaic Specialists Conference (PVSC)* (2016).
23. L. Chen, X. Chen, Y. Liu, Y. Zhao, X. Zhang, *J. Semicond,* **38**, 054005 (2017).
24. X. Zeng, X. Wen, X. Sun, W. Liao, Y. Wen, *Thin Solid Films* **605**, 257 (2016).
25. M.A. Gluba, N.H. Nickel, K. Hinrichs, J. Rappich, *J. Appl. Phys.* **113**, 043502 (2013).
26. S. Baturay, Y.S. Ocak, D. Kaya, *J. Alloys Compd.* 645 (2015).
27. H. Belaid, M. Noiri, Z. Ben Ayadi, K. Djessas, L. El Mir, *Energy Proc.* **84**, 214 (2015).
28. F.D. Auret S.A. Goodman, M.J. Legodi, W.E. Meyer, *Appl. Phys. Lett.* **80**, 1340 (2002).
29. M. Burgelman, P. Nollet, S. Degrave, *Thin Solid Films* **361-362**, 527 (2000).